



Research article

In-situ preparation of CoFe₂O₄ nanoparticles on eggshell membrane-activated carbon for microwave absorption

Hassan Soleimani^{a,**}, Jemilat Yetunde Yusuf^{a,*}, Lee Kean Chuan^a,
Hojjatollah Soleimani^b, Mustapha Lutfi bin Sabar^a, Andreas Öchsner^c,
Zulkifly Abbas^d, Asmau Iyabo Balogun^a, Gregory Kozlowski^{e,f}

^a Fundamental and Applied Science Department, Universiti Teknologi PETRONAS, 32610, Bandar Seri Iskandar, Perak, Malaysia

^b Department of Physics, North Tehran Branch, Islamic Azad University, 16511- 53311, Tehran, Iran

^c Faculty of Mechanical Engineering, Esslingen University of Applied Sciences, Kanalstrasse 33, 73728, Esslingen, Germany

^d Department of Physics, Faculty of Science, Universiti Putra Malaysia, UPM Serdang, Selangor Darul Ehsan, 43400, Malaysia

^e Geoscience Department, Universiti Teknologi PETRONAS, 32610, Bandar Seri Iskandar, Perak, Malaysia

^f Physics Department, Wright State University, Dayton, OH, 45435, United States



ARTICLE INFO

Keywords:

Electromagnetic waves
Carbon
Cobalt ferrite
Carbonization and microwave absorption

ABSTRACT

This study explores the potential of using cobalt ferrite (CF) nanoparticles grown in situ on eggshell membranes (ESM) to mitigate the increasing problem of electromagnetic interference (EMI). A simple carbonization process was adopted to synthesize CF nanoparticles on ESM. The study further examines the composites' surface morphology and chemical composition and evaluates their microwave absorption performance (MAP) at X-band frequency. Results showed that the composite of CF and ESM - CESM@CF, exhibited a strong RL peak value of -39.03 mm with an optimal thickness of 1.5 mm. The combination of CF and ESM demonstrates excellent impedance matching and EM wave attenuation. The presence of numerous interfaces, conduction loss from the morphology, interfacial polarisation, and dual influence from both CF and ESM contribute to the high MAP of the composite. CESM@CF composite is projected as an excellent biomass-based nano-composite for EM wave absorption applications.

1. Introduction

Electromagnetic radiation has become a primary global concern due to the environmental pollution arising from the extensive usage of wireless communication and electronic appliances in our everyday lives, endangering human health and substantially impeding the regular performance of some electric gadgets [1–5]. To overcome the problem of EMI, researchers have been working tirelessly to produce effective microwave absorption materials [6,7]. Microwave absorbers (MA) should have significant absorption ability, be lightweight, have wide absorption bandwidth, have a small thickness, have non-laborious, inexpensive cum simple synthesis procedures and have good thermal stability to suit the growing demand for practical applications [8–10]. Metal powders, metallic oxides, ferrites, and other magnetic materials have all been extensively studied in MA applications. Metallic oxides such as Fe₃O₄, Co₃O₄, and CoFe₂O₄ have greater complex permittivity and complex permeability features than other materials, resulting in better

* Corresponding author.

** Corresponding author.

E-mail addresses: hassan.soleimani@utp.edu.my (H. Soleimani), jemilatyus@yahoo.com (J.Y. Yusuf).

<https://doi.org/10.1016/j.heliyon.2023.e13256>

Received 20 July 2022; Received in revised form 21 January 2023; Accepted 23 January 2023

Available online 15 February 2023

2405-8440/© 2023 The Authors. Published by Elsevier Ltd. This is an open access article under the CC BY-NC-ND license (<http://creativecommons.org/licenses/by-nc-nd/4.0/>).

IMPMP characteristics [11–13].

On the other hand, metallic oxides are constantly hampered by their elevated specific gravity, restricted absorption bandwidth, poor IMPMP, high density, and effective absorption bandwidth [14,15]. On the other hand, microwave absorption materials made of Carbon provide several benefits, including lightweight, excellent electrical conductivity, and good stability [16,17]. Recent research has found that carbon materials with porous structures have been discovered to have significant EM wave absorption capability. Carbon-based materials (like carbon nanotubes (CNTs) and graphene) have been extensively utilized in EM wave absorption applications due to their exceptional dielectric loss capabilities [18,19]. Also, they possess good thermal stability, are low in weight, and have better electrical and mechanical properties, which are essential for enhanced EM wave absorption [20,21]. The creation of new types of EM wave absorption materials has emerged from the combination of carbon-based materials with magnetic materials, e.g., $\text{Li}_{0.3}\text{Zn}_{0.3}\text{Co}_{0.1}\text{Fe}_{2.3}\text{O}_4$ @MWCNT [22], CoFe_2O_4 hollow sphere with carbon spheres template [23], Co and Ni-doped Fe_2O_4 /RGO nanocomposite [24], CoFe_2O_4 /rGO porous nanocomposite [25] and Ni@Co/CNT@Ppy [26]. However, their laborious synthesis and high processing cost limit their use [27].

The use of Activated Carbon (AC) generated from biomass as a dielectric loss material has shown promising results in recent years [16]. The mesopores and micropores in AC offer a mix of solids and vacuum, allowing them to function as a suitable medium for improved IM [28,29]. Besides their lightweight, good thermal stability, simple and inexpensive preparation methods make them the right candidate for EM absorption applications [30,31]. Several microwave-absorbing materials have been developed by integrating the AC obtained from biomass with magnetic loss materials. For instance, a pine nutshell-derived AC/NiO nanoflake absorber was prepared by Wang et al. [32], and a minimum Reflection loss (RL) of -33.8 dB was achieved at a 6 mm absorber thickness. In another study by Sun et al. [33], a $\text{Ni}_{0.5}\text{Co}_{0.5}\text{Fe}_2\text{O}_4$ decorated AC (pomelo peel) absorber was fabricated. The composite exhibited a good MAP with an RL peak of -41.6 dB with an effective absorption bandwidth (EAB) of 4.3 GHz. The skeleton structure enhanced IM by boosting absorber attenuation through Debye relaxation, numerous reflections, and scattering, improving IM. The MAP of Coffee waste-derived bio-carbon/ MnFe_2O_4 composites was studied by Hassan et al. [2]. An enhanced minimum RL was achieved from -7.07 dB to -38.80 dB at a sample's thickness of 2.5 mm and an EAB of 3.5 GHz. The MAP of AC (coconut shell) loaded with magnetic FeO_x nanoparticles was reported by Wang et al. [34], with a minimum RL peak of -29.5 dB at an absorber thickness of 2.7 mm and EAB of 6.4 GHz. Further studies also reveal that adding biomass-derived AC significantly improved the absorption performance of magnetic metal and their oxides. For example, the AC (banana peel)/ Co_3O_4 absorber prepared by Yusuf et al. [35] showed an outstanding RL of -51.5 dB at 2.5 mm thickness. Thair et al. [36] also designed a Co/ Fe_2O_3 /AC with RL peak of -69.39 dB at 11.19 GHz at an absorber thickness of 3 mm with 15% filler loading. In addition, Hu et al. [27] also synthesized biomass-derived carbon/ NiCo_2S_4 with an RL peak of -62.74 dB at 2.24 mm thickness. The absorber showed a good absorption bandwidth of 7.62 GHz at an absorber thickness of 1.96 mm.

This work used CF nanoparticles as the magnetic loss material due to their chemical stability, good magnetic saturation, and mechanical hardness [37]. ESM was used as the precursor for the dielectric material due to its availability and low cost. Using a simple carbonization technique, the CF nanoparticles were grown in situ on the carbonized eggshell membrane (CESM) and uncarbonated eggshell membrane (UCESM). The samples were labeled CF, CESM@CF, and UCESM@CF composite, respectively. The UCESM@CF composites achieved an RL peak of -39.03 dB at 10.44 GHz, compared to pure CF, owing to a low filler loading ratio of 20% and a thin matching thickness of 2.0 mm. As a result, the CESM@CF composite can be a good choice for ultralight, high-efficiency microwave absorbers.

2. Methodology

2.1. Material

ESM, $\text{Fe}(\text{NO}_3)_3 \cdot 9\text{H}_2\text{O}$, $\text{Co}(\text{NO}_3)_2 \cdot 6\text{H}_2\text{O}$, NaOH, Citric acid, Ethanol, Distilled water, and Paraffin wax. All the chemicals acquired from R&M chemicals Malaysia were of analytical grade.

2.2. Preparation of carbonized eggshell membrane (CESM)

The ESM were rinsed with hot and cold water to remove the impurities. Then, the ESM were vacuum dried at 80°C for 12 h. 10 g of the dried ESM was carbonized at 800°C in a tube furnace with a ramping rate of $5^\circ\text{C}/\text{min}$ for 1 h under steady nitrogen flow. The obtained carbonized ESM was labeled CESM, and the remaining dried ESM was labeled as uncarbonated ESM (UCESM).

2.3. Synthesis cobalt ferrite (CF)

1:2 ratio of $\text{Co}(\text{NO}_3)_2$ and $\text{Fe}(\text{NO}_3)_3$ were dissolved in 30 mL of distilled water under vigorous stirring for 30 min. 2.0 M of an aqueous solution of NaOH was added drop-wise into the dissolved $\text{Co}(\text{NO}_3)_2$ and $\text{Fe}(\text{NO}_3)_3$ solution to maintain the pH. The pH was maintained in the range of 9–10. Then, the mixture was heated at 60°C on a hot plate stirrer for an hour. The formation of the precipitate was observed afterwards, and the precipitate was filtered. The filtered product was washed with distilled water and dried at 80°C in a vacuum oven. The dried product was finally calcined at 500°C for 1 h in a tube furnace ($5^\circ\text{C}/\text{min}$) and allowed to cool naturally. The product was then collected, stored in an airtight container, and labeled CF.

2.4. Preparation of Cobalt Ferrite and Carbonized Eggshell Membrane (CESM@CF) and Cobalt Ferrite and Uncarbonized Eggshell Membrane (UCESM@CF) nanocomposites

First, The cobalt ferrite solution was prepared by dissolving 1 M of $\text{Co}(\text{NO}_3)_2 \cdot 6\text{H}_2\text{O}$, 2 M $\text{Fe}(\text{NO}_3)_3 \cdot 9\text{H}_2\text{O}$ in 15 mL ethanol, and 7 mL deionized water. 3.0 g citric acid was added, and the mixture was stirred vigorously to obtain a homogeneous solution. Then, 1 g of CESM was immersed into 20 mL of the prepared CoFe_2O_4 solution and labeled CESM@CF. Also, 1 g of the dried uncarbonized eggshell membrane (UCESM) was immersed in 20 mL of the CoFe_2O_4 solution and labeled UCESM@CF. Both samples were allowed to dry naturally (complete evaporation). The samples were finally calcined at 800°C in an inert environment (See Fig. 1).

2.5. Characterization

The nanocomposites' surface morphology was studied using Zeiss (Supra V55) Field Emission Scanning Electron Microscopy (FESEM) at 20 kV. Energy Dispersive X-ray (EDX) spectroscopy was used to estimate elemental distribution. All samples' functional groups and chemical bonding were analyzed using a PerkinElmer (Frontier 01) FT-IR spectrometer. The IR spectrum was studied in the range of $4000\text{--}400\text{ cm}^{-1}$, and the KBr method was used during the FTIR analysis. The samples' crystalline structure and phase analysis were investigated using the Panalytical Xpert 3 Powder X-ray Diffractometer (XRD) (20° to 80°). The surface area and porosity (SAP) study was performed using a Micromeritics (Tristar II 3020) surface area and porosity analyzer.

2.6. Microwave absorption characterization

The samples' electromagnetic properties, i.e., μ_r (the complex permeability) and ϵ_r (complex permittivity), were measured using a Vector Network Analyzer. The samples were filled in 30 wt% paraffin wax and molded into a rectangular shape for EM measurement. The MAP was calculated based on equations (1) and (2).

$$Z_{in} = Z_0 \sqrt{\frac{\mu_r}{\epsilon_r}} \tan h \left(j \frac{2\pi f d}{c} \sqrt{\epsilon_r \mu_r} \right) \quad 1$$

$$RL(\text{dB}) = 20 \log_{10} |\Gamma| \quad 2$$



Fig. 1. Flowchart diagram for preparation of CESM@CF and UCESM@CF Nanocomposite.

3. Results & discussion

XRD was used to ascertain the crystalline structure and phase identification of the samples, and the diffraction pattern is presented in Fig. 2a. The Bragg diffraction peak of 2θ at 18.73° , 29.58° , 36.2° , 43.02° , 48.0° , 54.09° , 57.84° , 63.84° , and 77.3° represent the (111), (220), (311), (222), (400), (422), (511), and (440) planes of the CF with face-centred cubic spinel structure [38]. The carbon peaks were not visible in the UCESM@CF and CESM@CF due to the amorphous nature or presence of distorted Carbon. Besides the *in-situ* growth of CF nanoparticles on the ESM surface, it can also result in low crystallinity of Carbon in UCESM@CF and CESM@CF samples. From the XRD analysis, it can be concluded that all samples have a cubic crystal structure. Fig. 2b shows the FTIR spectra of the samples. A broad peak between 3400 and 3440 cm^{-1} corresponding to O–H bending was observed in all the samples due to the adsorbed water [39]. A sharp peak was found at 1392.5 cm^{-1} in the CF sample, which corresponds to the COO⁻ anti-symmetric stretching vibration [40]. Three peaks were observed at 802.40 cm^{-1} , 640 cm^{-1} , and $464\text{--}474\text{ cm}^{-1}$, representing the M – O stretching vibration of Co^{2+} ions in tetrahedral voids, Fe^{3+} ions in tetrahedral voids, and octahedral respectively [41]. Due to the presence of ESM, some peaks were only observed in UCESM@CF and CESM@CF. These peaks include a weak peak at 2916 cm^{-1} (C–H) and another peak at $2340\text{--}2424\text{ cm}^{-1}$ (C–H stretching vibration) [42]. A C–O bending vibrations modes peak was also observed at 1070 cm^{-1} and an aromatic stretching vibration of the C=O at $1719\text{--}1716\text{ cm}^{-1}$. In both CESM@CF and UCESM@CF, a weak C=C aromatic group was observed at 1528 cm^{-1} . Additionally, the peak observed between 1448 and 1485 cm^{-1} in CESM@CF corresponds to C=C which could be ascribed to the two-time carbonization for the CESM@CF [39]. The FTIR analysis confirms the successful doping of CF on ESM as well as the carbonization process of ESM.

The structure of the UCESM@CF and CESM@CF nanocomposite was investigated using FESEM. The FESEM image of both UCESM@CF and CESM@CF nanocomposite can be seen in Fig. 3a&b and Fig. 3c&d. The CESM@CF nanocomposite revealed the presence of well-developed pores compared to the UCESM@CF nanocomposite (Fig. 3c&d). This could be ascribed to the dual carbonization in CESM@CF (Fig. 3a&b). CESM@CF and UCESM@CF showed a porous skeleton structure on which the CF nanoparticles are grafted to the surface. From the FESEM images, it can be concluded that the CF nanoparticles were well distributed on the surface of the CESM, as shown by the elemental mappings of the CESM@CF and UCESM@CF nanocomposites in Fig. 4.

The Energy Dispersive X-Ray Spectroscopy (EDS) showed the composition of the elements in the nanocomposites. Fig. 4a–h shows the EDS mapping of both nanocomposites. Based on the figure, the cobalt (Co), iron (Fe), oxygen (O), and carbon (C) elements are

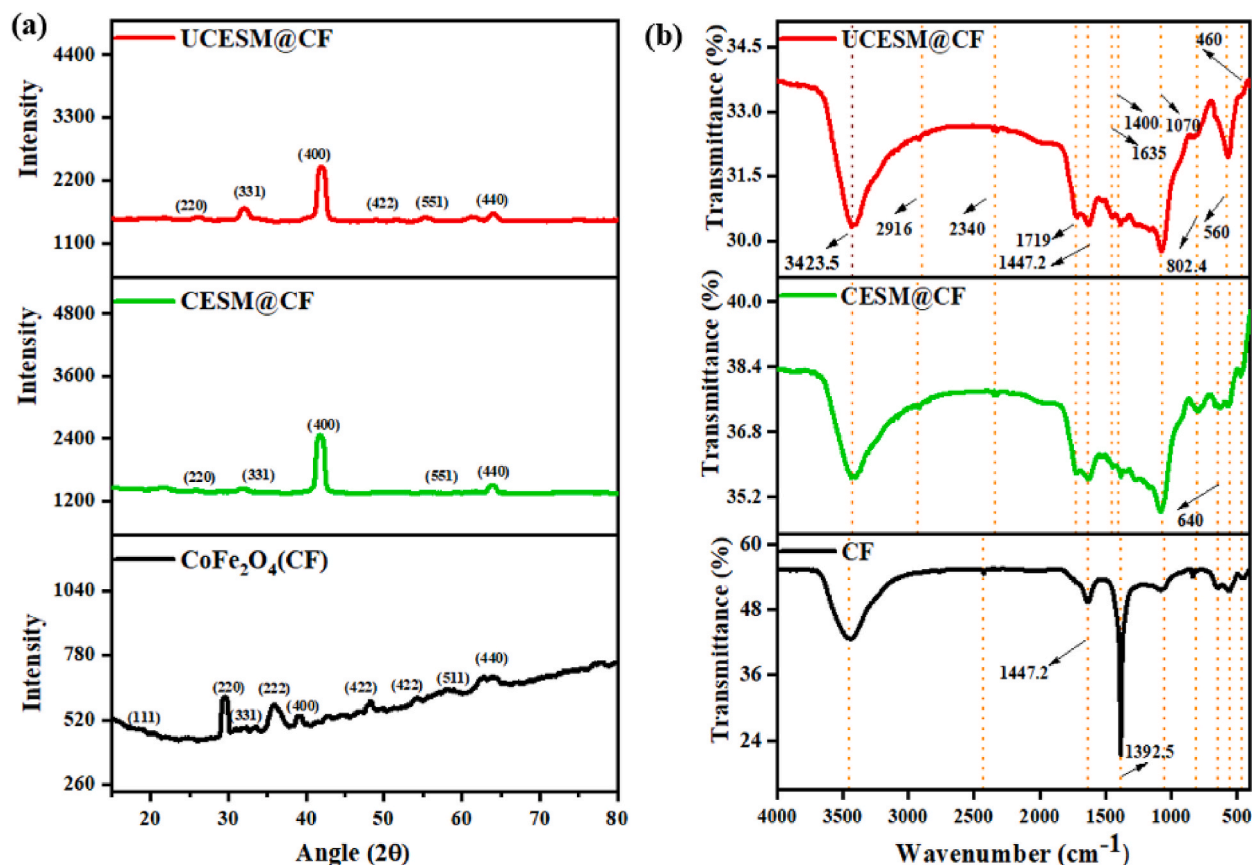


Fig. 2. (a): XRD diffraction and (b): FTIR Spectra of CF, UCESM@CF, and CESM@CF

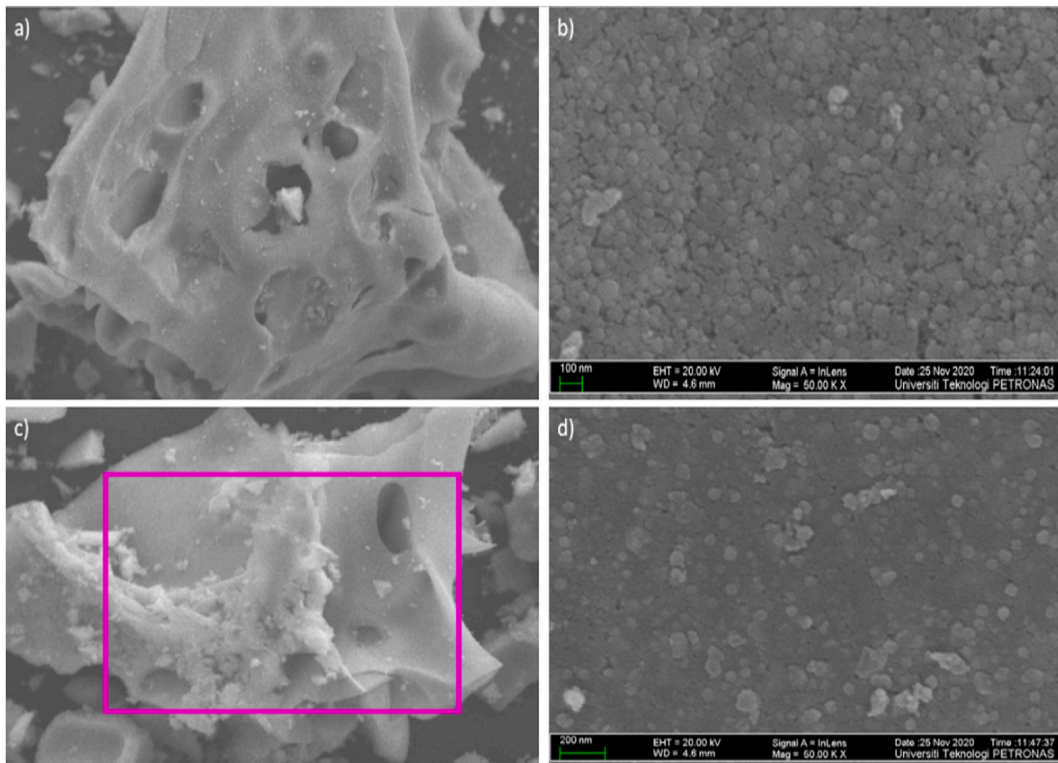


Fig. 3. FESEM image of samples (a–b) CESH@CF (c–d) UCESH@CF nanocomposites.

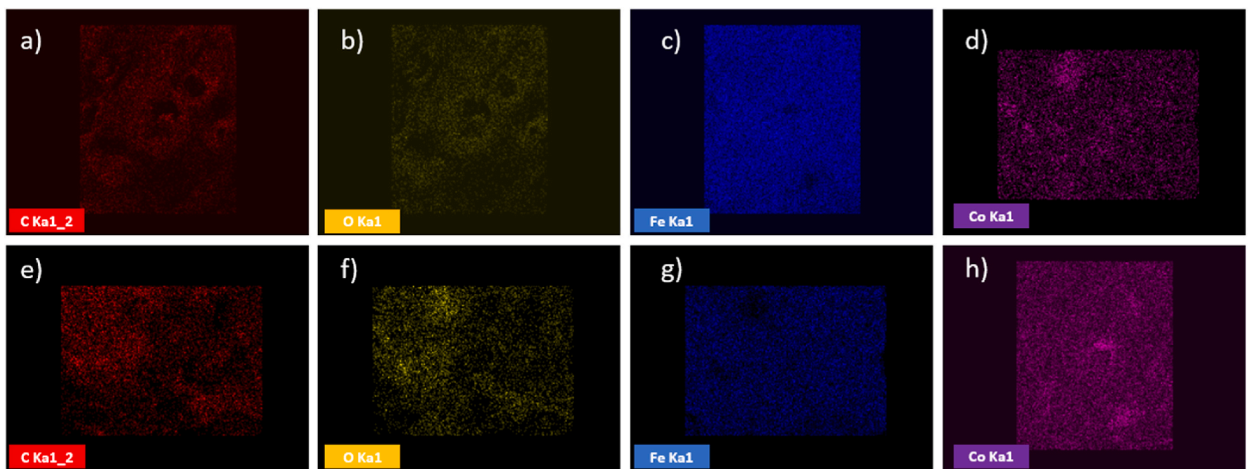


Fig. 4. Elemental mapping of composite samples (a–d) CESH@CF (e–h) UCESH@CF nanocomposites.

uniformly distributed throughout the surface of both nanocomposites.

Fig. 5 represents the N₂ desorption and adsorption isothermal analysis of CF, CESH@CF, and UCESH@CF samples. CF showed a type IV isotherm with a hysteresis loop (Fig. 5a). The isotherm curves of CESH@CF and UCESH@CF are similar (Fig. 5b&c). CESH@CF shows maximum Nitrogen adsorption and also exhibits a large surface area. The increasing trend in the CESH@CF surface area is due to the dual carbonization during the sample preparation. As observed in Fig. 5b&c, CESH@CF and UCESH@CF show a type II isotherm with an H₃ hysteresis loop showing the existence of both mesopores and micropores in the sample. The sharp rise in nitrogen uptake illustrates mesoporous structures' presence [38]. The pore distribution and pore volume are shown in Table 1. The presence of special inner cavities and high surface area with relatively small pores will be beneficial for trapping EM waves thereby resulting in interfacial polarisation due to the development of abundant interfaces and junctions at the surface of the samples [13].

The MAP of the samples is further analyzed by studying the electromagnetic parameters; $\mu_r = \mu' - j\mu''$ and $\epsilon_r = \epsilon' - j\epsilon''$. The ϵ' and

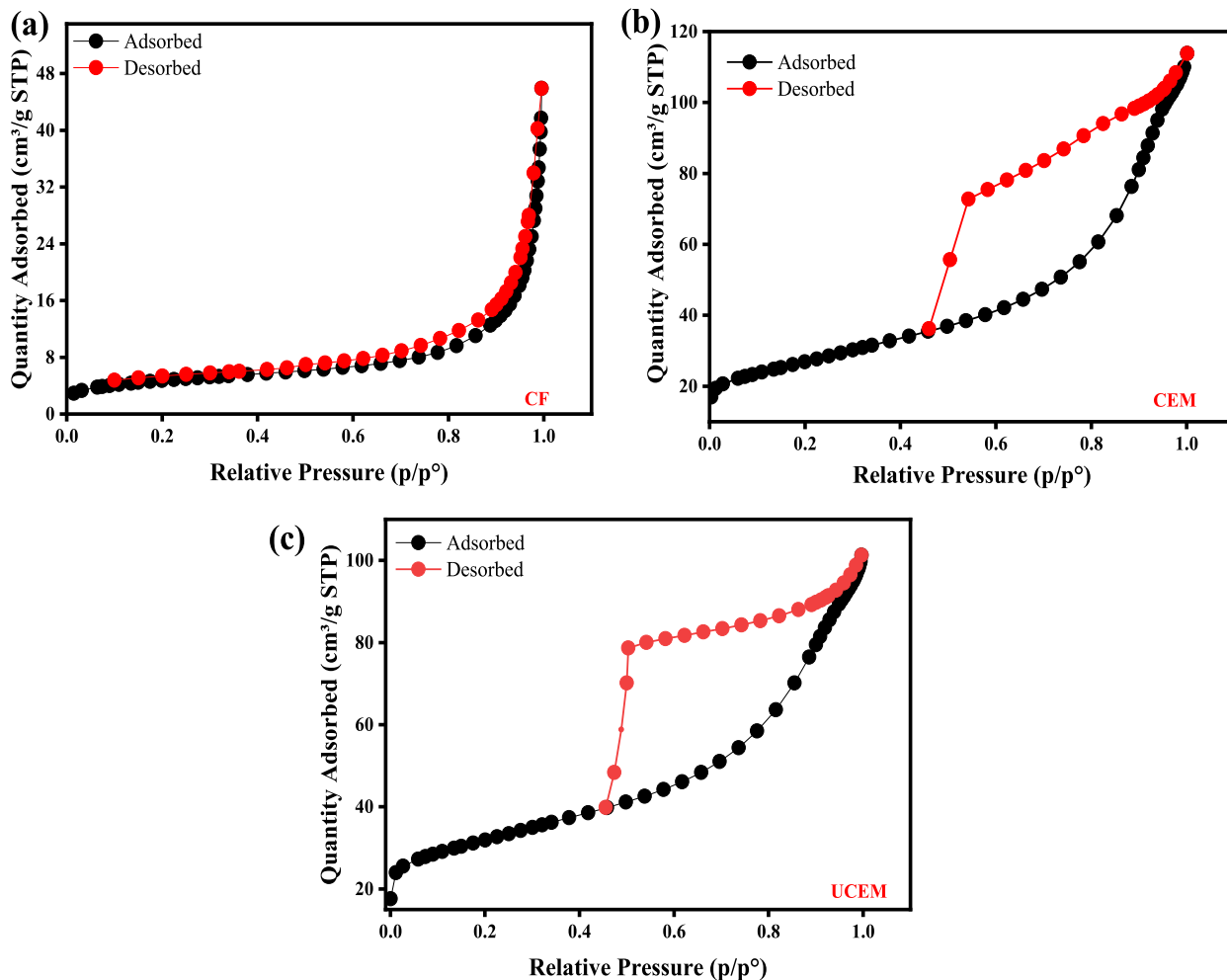


Fig. 5. Nitrogen-desorption and adsorption curve for (a) CF (b) CESM@CF and (c) UCESM@CF

Table 1
Pore and surface area distribution of CF, UCESM@CF, and CESM@CF

Sample	BET Surface Area (m^2/g)	Total Pore Volume ($cm^3 g^{-1}$)	Average Pore Size (nm)
CoFe ₂ O ₄	44.6593	0.061503	10.09
UCESM@CF	93.0915	0.1293–0.1747	5.72
CESM@CF	107.4590	0.1520–0.1641	7.32

μ' measure the ability of the sample to store dielectric and magnetic energy, while the e'' and μ'' measure the ability of the sample to dissipate magnetic and electric energy. The dielectric loss tangent ($\tan \delta_e = e''/e'$) and magnetic loss tangent ($\tan \delta_\mu = \mu''/\mu'$) measures the power loss ability of the sample.

Fig. 6a shows the real and imaginary permittivity of the samples decreases as the frequency increases. The e' for CF fluctuates across the X band frequency. Whereas the e'' also fluctuates across the whole frequency. It is an established fact that complex permittivity is derived from electronic polarisation, interfacial polarisation, and ionic polarisation, which are significantly influenced by structure and surface morphology [43]. Thus, the high values e' and e'' in UCESM@CF and CESM@CF may be attributed to the typical frequency dispersion characteristic resulting from carbon [43,44]. In addition, the porous structure and large surface area, which was corroborated by the FESEM image and SAP distribution (Table 1), can result in increased charge transport and interfacial polarisation.

Fig. 6b shows the μ' and μ'' of the CF, UCESM@CF, and CESM@CF samples. The μ' for CF fluctuates across the studied frequency, whereas the μ'' of CF increases to 0.181 due to the uncompensated moments in the CF nanostructure sample. Also, defects such as strains and stacking faults at the interface contributed to the μ'' . The addition of Carbon reduced the magnetic performance of the CF. This account for the low values of μ' and μ'' in UCESM@CF and CESM@CF samples across the frequency range. Eddy current loss, natural resonance, and exchange resonance are attributes of the magnetic loss mechanism in microwave absorption. From Fig. 6c, it

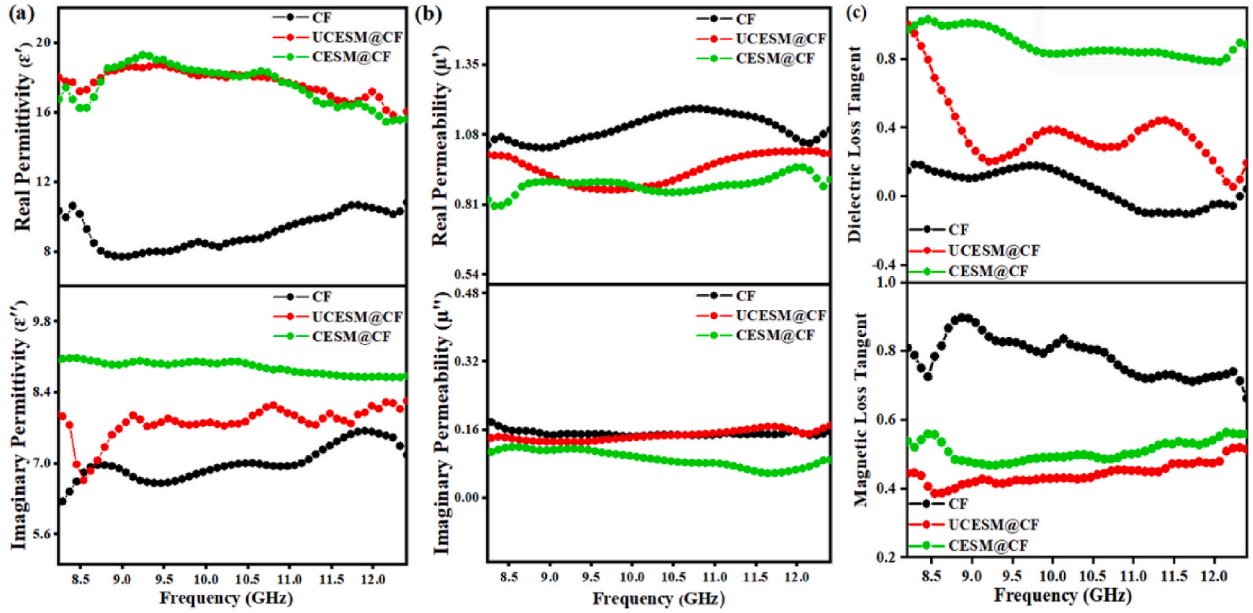


Fig. 6. (a) Real & Imaginary Permittivity of CF, UCESM@CF, and CESM@CF (b) Real and Imaginary permeability of CF, UCESM@CF, and CESM@CF (c) Dielectric and magnetic loss tangents of CF, UCESM@CF, and CESM@CF

was observed that the CESM@CF and UCESM@CF have much higher dissipation ability compared to the CF. The magnetic loss tangents of CF were higher compared to the composites. This suggests that dielectric loss significantly impacts the MAP of both the CESM@CF and UCESM@CF absorbers. In addition, the porous morphology of the CESM@CF and UCESM@CF allowed the incoming wave to be trapped in the cavity of the samples, resulting in multiple reflections and multiple scattering of EM waves [45]. The MAP of the samples is evaluated via RL, which can be calculated based on equations (1) and (2). An absorption performance below -10 dB indicates that the material has attenuated 90% of the EM wave. Whereas RL below -20 dB denotes that the material has absorbed more than 98% of the EM wave. The RL values of the samples were simulated at varying thicknesses to determine their MAP.

Fig. 7 shows the RL curve for the samples at 20 wt% loadings with paraffin as a function of frequency for different absorber thicknesses. With increasing thickness, the sample's absorption maxima move to a lower frequency range, followed by attenuation in lower frequency bands. The $\frac{1}{4}$ wavelength equation [60] helps explain the changing peaks.

$$t_m = \frac{nc}{4f_m} (\epsilon_t \mu_t)^{\frac{1}{2}} \tag{3}$$

where t_m denotes the matching thickness, f_m symbolizes the matching frequency, and c is the velocity of light. As observed in Fig. 7a, a minimum RL of -41.35, -42.37, and -53.20 dB was obtained for CF nanoparticles at 11.16, 9.8, and 8.56 GHz with a thickness of 3.5, 4.0, and 4.5 mm respectively. The combination of CF and ESM greatly reduced the thickness of the absorber, which is one of the unique properties of an ideal MA. UCESM@CF possess a minimum RL of -37.26, -39.13, and -46.87 dB at 11.32, 9.76, 8.56 GHz respectively with an effective absorption bandwidth of 0.53, 1.46 and 1.55 GHz at 2.0 mm, 2.5 mm and 3.0 mm thickness respectively (Fig. 7b). The CESM@CF (Fig. 7c) showed an outstanding MAP with an absorber thickness of 1.5 mm, 1.9 GHz EAB, and a minimum RL of -39.03 dB. It also showed good absorption with RL = -34.67 dB at a thickness of 2.0 mm. The results suggest that the CESM@CF sample can be used as an ideal and promising EM wave absorber due to its excellent microwave absorption at a thin thickness and low density (20 wt %).

$$(\epsilon' - \epsilon_\infty)^2 + \epsilon''^2 = (\epsilon_s - \epsilon_\infty)^2 \tag{4}$$

The Debye polarisation relaxation phenomenon is a well-known way of explaining dielectric loss processes. The ϵ' and ϵ'' fulfill equation (4), and the ϵ' vs. ϵ'' displays a semicircular ring, according to Debye theory. Fig. 7d presents the Cole-Cole curve for CF, UCESM@CF, and CESM@CF. All the samples possess more than one semicircle, as indicated with a stroke, implying that the samples exhibit multiple dybe relaxation processes. As observed in Fig. 7d the number of semicircles present in CESM@CF samples increases compared to CF and UCESM@CF due to ESM (Carbon) in the composite. Thus, indicating that interfacial polarisation or defects in the composites contribute to the dielectric loss of the CESM@CF sample. CESM and UCESM@CF have good conductivity and conduction networks, a significant contributor to dielectric loss. The presence of long-tail in UCESM can be attributed to conduction loss.

Fig. 8a-c shows that as the matching thickness (t_m) increases the frequency shifts gradually toward the low frequency. At 8.72 GHz, the minimum RL is 47.3 dB, or 2.4 mm of matching thickness. The RL of CF, CESM@CF and UCESM@CF reaches the peak value if the t_m and f_m satisfy the abovementioned equation (3). Thus, Fig. 8 shows that the samples obey the $\frac{1}{4}$ cancellation model and exhibit

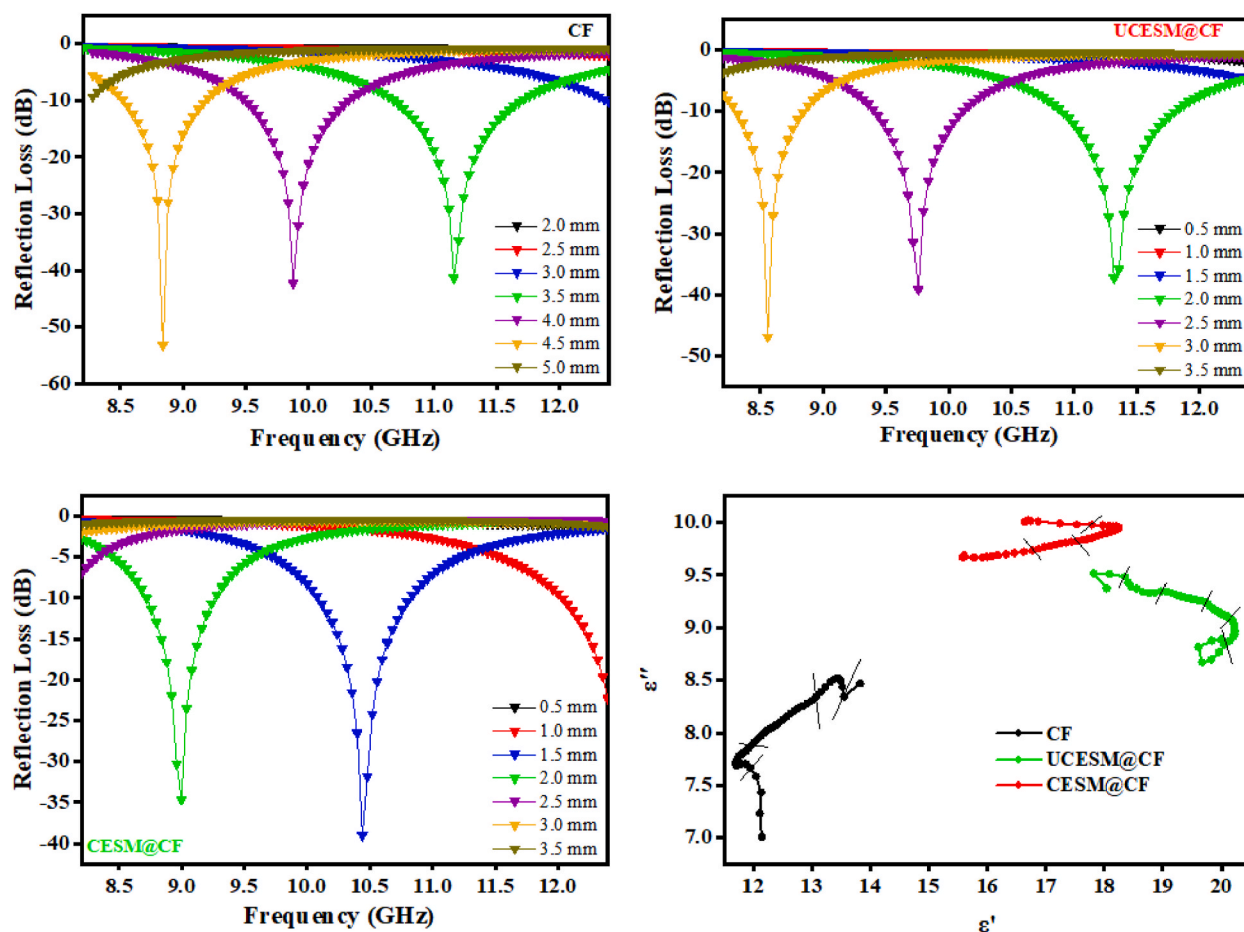


Fig. 7. (a)–(c): 2D graph of RL over X-band frequency range (d) Cole-Cole plot of the samples.

good absorption performance.

4. Conclusion

In conclusion, a simple carbonization method was used to fabricate a lightweight, low-cost ESM@CF absorber with good morphology. The CoFe_2O_4 NPs increased CESM's EM wave absorption capacities from 10.1 to 49.6 dB at 9.2 GHz and showed an increased EAB, owing to the synergetic impact of CF and ESM. The coupling of CF nanoparticles with ESM reduces the saturation magnetization of the CESM@CF and UCESM@CF composites due to the weak magnetic properties of Carbon. Furthermore, simulations of the CESM@CF and UCESM@CF nanocomposite absorbers show that nanocomposites possess greater capacity to attenuate powerful incident EM waves. At 20 wt% filler loading, the CESM@CF and UCESM@CF composites display exceptional MAP, at an absorber thickness of 1.5 mm, and a minimum RL value of -39.03 dB at 10.44 GHz. The increased MAP is due to their unique morphology, a synergistic influence from both the ESM and CF, superior IMPM, and significant attenuation capabilities. Thus, eggshell membrane-derived composites are potential and promising absorbers for microwave absorption application and provide a novel strategy for fabricating carbon-based EM wave absorbers with intense absorption strength, wide absorption bandwidth, low filler loading, and thin thickness.

Author contribution statement

Hassan Soleimani: Conceived and designed the experiments. Jemilat Yetunde Yusuf: Analyzed and interpreted the data; Wrote the paper. Lee Kean Chuan, Zulkifly Abbas, Gregory Kozlowski: Contributed reagents, materials, analysis tools or data. Hojjatollah Soleimani, Andreas Öchsner, Asmau Iyabo Balogun: Analyzed and interpreted the data. Mustapha Lutfi bin Sabar: Performed the experiments.

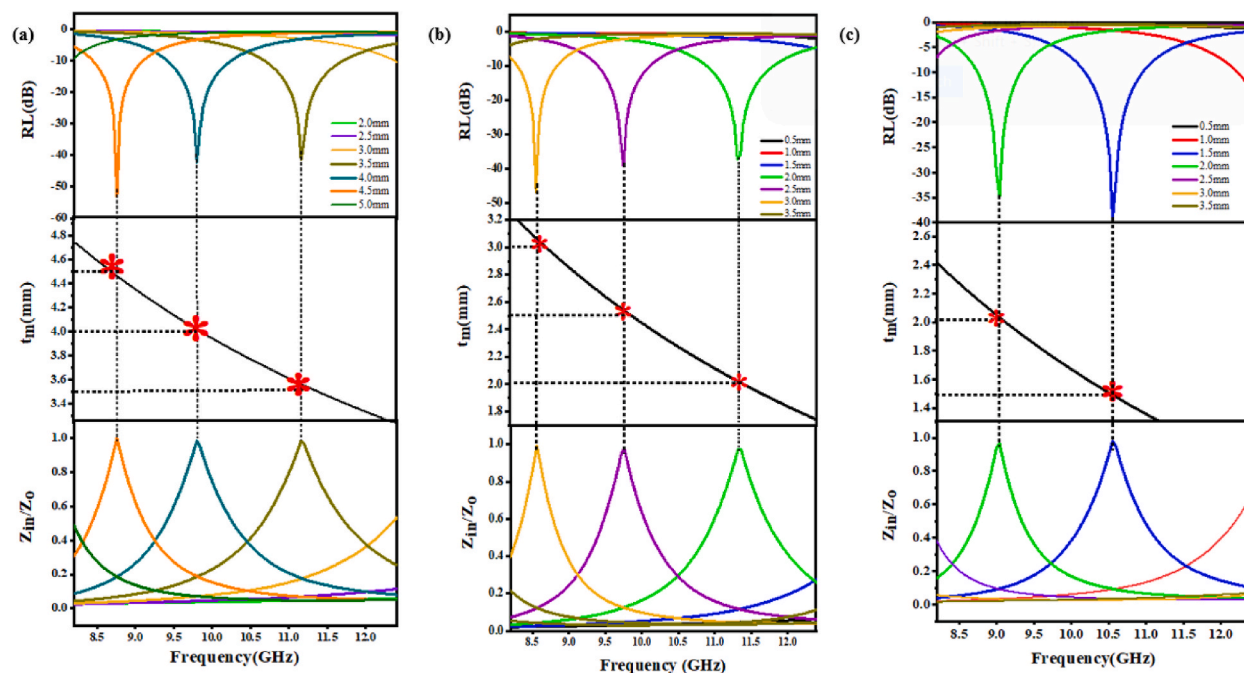


Fig. 8. RL-frequency curves and dependence of t_m (matching thickness) on f_m (matching frequency) under $\lambda/4$ conditions (a) CF (b) UCESM@CF and (c) CESM@CF

Funding statement

This work is supported by the Fundamental Research Grant Scheme (Ministry of Higher Education FRGS (015MA0-134) and the Yayasan Universiti of Teknologi Petronas Education grant (YUTP 015CL0-333) UTP, Perak, Malaysia.

Data availability statement

Data will be made available on request.

Declaration of competing interest

The authors declare no conflict of interest.

References

- [1] L. Chen, et al., In-situ pyrolyzed polymethylsilsesquioxane multi-walled carbon nanotubes derived ceramic nanocomposites for electromagnetic wave absorption, *Ceram. Int.* 45 (9) (2019) 11756–11764, <https://doi.org/10.1016/j.ceramint.2019.03.052>.
- [2] A. Hassan, W. Ding, M.A. Aslam, Y. Bian, Q. Liu, Z. Sheng, Microwave absorption property of coffee waste bio-carbon modified by industrial waste MnFe2O4 particles, *J. Mater. Res. Technol.* 9 (6) (2020/11/01/2020) 12869–12879, <https://doi.org/10.1016/j.jmrt.2020.09.015>.
- [3] H. Wei, et al., Multifunctions of polymer nanocomposites: environmental remediation, electromagnetic interference shielding, and sensing applications, *ChemNanoMat* 6 (2) (2020) 174–184, <https://doi.org/10.1002/cnma.201900588>.
- [4] C. Wang, et al., Overview of carbon nanostructures and nanocomposites for electromagnetic wave shielding, *Carbon* 140 (2018) 696–733, <https://doi.org/10.1007/s40820-019-0255-3>.
- [5] M. Ma, et al., 1D flower-like Fe3O4@SiO2/MnO2 nanochains inducing RGO self-assembly into aerogels for high-efficient microwave absorption, *Mater. Des.* 188 (2020), <https://doi.org/10.1016/j.matdes.2019.108462>.
- [6] P. Liu, et al., Core-shell Ni@C encapsulated by N-doped carbon derived from nickel-organic polymer coordination composites with enhanced microwave absorption, *Carbon* 170 (2020/12/01/2020) 503–516, <https://doi.org/10.1016/j.carbon.2020.08.043>.
- [7] P. Negi, A.K. Chhantyal, A.K. Dixit, S. Kumar, A. Kumar, Activated carbon derived from mango leaves as an enhanced microwave absorbing material, *Sustain. Mater. Technol.* 27 (2021), <https://doi.org/10.1016/j.susmat.2020.e00244>.
- [8] Y. Yu, et al., Tuning the inner hollow structure of lightweight amorphous carbon for enhanced microwave absorption, *Chem. Eng. J.* 375 (2019), 121914, <https://doi.org/10.1016/j.cej.2019.121914>.
- [9] S. Ayub, et al., Optimization of magnetite with Modified graphene for microwave absorption properties, *J. Alloys Compd.* (2022), 168182, <https://doi.org/10.1016/j.jallcom.2022.168182>.
- [10] F.A. Wahaab, et al., Graphene@Ni0.5Co0.5Fe2O4 hybrid framework with enhanced interfacial polarization for electromagnetic wave absorption, *J. Alloys Compd.* 854 (2021/02/15/2021), 157259, <https://doi.org/10.1016/j.jallcom.2020.157259>.
- [11] Y. Li, S. Li, T. Zhang, L. Shi, S. Liu, Y. Zhao, 3D hierarchical Co3O4/Reduced graphene oxide/melamine derived carbon foam as a comprehensive microwave absorbing material, *J. Alloys Compd.* 792 (2019) 424–431, <https://doi.org/10.1016/j.jallcom.2019.03.359>.

- [12] I. Abdalla, J. Shen, J. Yu, Z. Li, B. Ding, Co3O4/carbon composite nanofibrous membrane enabled high-efficiency electromagnetic wave absorption, *Sci. Rep.* 8 (1) (Aug 17 2018), 12402, <https://doi.org/10.1038/s41598-018-30871-2>.
- [13] L.L. Adebayo, et al., A simple route to prepare Fe3O4@C microspheres as electromagnetic wave absorbing material, *J. Mater. Res. Technol.* 12 (2021/05/01/2021) 1552–1563, <https://doi.org/10.1016/j.jmrt.2021.03.094>.
- [14] J.Y. Yusuf, H. Soleimani, Y.K. Sanusi, L.L. Adebayo, S. Sikiru, F.A. Wahaab, Recent advances and prospect of cobalt based microwave absorbing materials, *Ceram. Int.* (2020), <https://doi.org/10.1016/j.ceramint.2020.07.244>.
- [15] L.L. Adebayo, et al., Recent advances in the development OF Fe3O4-BASED microwave absorbing materials, *Ceram. Int.* 46 (2) (2020) 1249–1268, <https://doi.org/10.1016/j.ceramint.2019.09.209>.
- [16] H. Zhao, et al., Biomass-derived porous carbon-based nanostructures for microwave absorption, *Nano-Micro Lett.* 11 (1) (2019), <https://doi.org/10.1007/s40820-019-0255-3>.
- [17] Y.M. Manawi, A. Samara, T. Al-Ansari, M.A. Atieh, A review of carbon nanomaterials' synthesis via the chemical vapor deposition (CVD) method, *Materials* 11 (5) (2018) 822, <https://doi.org/10.3390/ma11050822>.
- [18] F. Meng, et al., Graphene-based microwave absorbing composites: a review and prospective, *Compos. B Eng.* 137 (2018) 260–277, <https://doi.org/10.1016/j.compositesb.2017.11.023>.
- [19] W. Xu, G.-S. Wang, P.-G. Yin, Designed fabrication of reduced graphene oxides/Ni hybrids for effective electromagnetic absorption and shielding, *Carbon* 139 (2018) 759–767, <https://doi.org/10.1016/j.carbon.2018.07.044>.
- [20] H.-B. Zhao, J.-B. Cheng, Y.-Z. Wang, Biomass-derived Co@crystalline carbon@carbon aerogel composite with enhanced thermal stability and strong microwave absorption performance, *J. Alloys Compd.* 736 (2018/03/05/2018) 71–79, <https://doi.org/10.1016/j.jallcom.2017.11.120>.
- [21] F.A. Wahaab, et al., Microwave absorption performance of Ni0.5Zn0.5Fe2O4 nanoclusters at 8.2–18 GHz frequency, *Indian J. Phys.* 96 (3) (2022/03/01 2022) 723–733, <https://doi.org/10.1007/s12648-021-02005-4>.
- [22] M. Dalal, et al., Microwave absorption and the magnetic hyperthermia applications of Li0.3Zn0.3Co0.1Fe2.3O4 nanoparticles in multiwalled carbon nanotube matrix, *ACS Appl. Mater. Interfaces* 9 (46) (2017/11/22 2017) 40831–40845, <https://doi.org/10.1021/acsami.7b12091>.
- [23] J. Zhou, R. Tan, Z. Yao, H. Lin, Z. Li, Preparation of CoFe2O4 hollow spheres with carbon sphere templates and their wave absorption performance, *Mater. Chem. Phys.* 244 (2020), 122697, <https://doi.org/10.1016/j.matchemphys.2020.122697>.
- [24] A. Das, P. Negi, S.K. Joshi, A. Kumar, Enhanced microwave absorption properties of Co and Ni co-doped iron (II, III)/reduced graphene oxide composites at X-band frequency, *J. Mater. Sci. Mater. Electron.* 30 (21) (2019) 19325–19334, <https://doi.org/10.1007/s10854-019-02293-x>.
- [25] Y. Liu, et al., Broadband and lightweight microwave absorber constructed by in situ growth of hierarchical CoFe2O4/reduced graphene oxide porous nanocomposites, *ACS Appl. Mater. Interfaces* 10 (16) (2018/04/25 2018) 13860–13868, <https://doi.org/10.1021/acsami.8b02137>.
- [26] Y. Bi, et al., One-dimensional Ni@Co/C@PPy composites for superior electromagnetic wave absorption, *J. Colloid Interface Sci.* 605 (2022) 483–492, <https://doi.org/10.1016/j.jcis.2021.07.050>.
- [27] P. Hu, S. Dong, X. Li, J. Chen, P. Hu, Flower-like NiCo2S4 microspheres based on nanosheet self-assembly anchored on 3D biomass-derived carbon for efficient microwave absorption, *ACS Sustain. Chem. Eng.* 8 (27) (2020/07/13 2020) 10230–10241, <https://doi.org/10.1021/acssuschemeng.0c03013>.
- [28] Z. Wu, et al., Hierarchically porous carbons derived from biomasses with excellent microwave absorption performance, *ACS Appl. Mater. Interfaces* 10 (13) (2018/04/04 2018) 11108–11115, <https://doi.org/10.1021/acsami.7b17264>.
- [29] P. Negi, S.K. Joshi, H.B. Baskey, S. Kumar, A.K. Mishra, A. Kumar, Excellent microwave absorbing performance of biomass-derived activated carbon decorated with in situ-grown CoFe2O4 nanoparticles, *Mater. Adv.* (2022), <https://doi.org/10.1039/D1MA01116B>, 10.1039/D1MA01116B.
- [30] J.Y. Yusuf, et al., Electromagnetic Wave Absorption of Coconut Fiber-Derived Porous Activated Carbon, *Boletín de la Sociedad Española de Cerámica y Vidrio*, 2021, <https://doi.org/10.1016/j.bsecv.2021.02.003>.
- [31] H. Soleimani, J.Y. Yusuf, H. Soleimani, L.K. Chuan, M. Sabet, Banana-peel derived activated carbon for microwave absorption at X-band frequency, *Synth. Sinter.* 2 (3) (2022) 120–124, <https://doi.org/10.53063/synsint.2022.2389>.
- [32] H. Wang, et al., Biomass carbon derived from pine nut shells decorated with NiO nanoflakes for enhanced microwave absorption properties, *RSC Adv.* 9 (16) (2019) 9126–9135, <https://doi.org/10.1039/C9RA00466A>.
- [33] J. Sun, J. Chen, H. Ge, H. Sun, Y. Yang, Y. Zhang, Biomass-derived carbon decorated with Ni0.5Co0.5Fe2O4 particles towards excellent microwave absorption performance, *Compos. Appl. Sci. Manuf.* 156 (2022/05/01/2022), 106850, <https://doi.org/10.1016/j.compositesa.2022.106850>.
- [34] L. Wang, H. Guan, S. Su, J. Hu, Y. Wang, Magnetic FeOX/biomass carbon composites with broadband microwave absorption properties, *J. Alloys Compd.* 903 (2022/05/15/2022), 163894, <https://doi.org/10.1016/j.jallcom.2022.163894>.
- [35] J.Y. Yusuf, H. Soleimani, L.K. Chuan, Y.K. Sanusi, L.L. Adebayo, Physicochemical properties and microwave absorption performance of Co3O4 and banana peel-derived porous activated carbon composite at X-band frequency, *J. Alloys Compd.* 888 (2021), 161474, <https://doi.org/10.1016/j.jallcom.2021.161474>. /12/25/2021.
- [36] D. Tahir, et al., Excellent electromagnetic wave absorption of Co/Fe2O3 composites by additional activated carbon for tuning the optical and the magnetic properties, *J. Alloys Compd.* 864 (2021), 158780, <https://doi.org/10.1016/j.jallcom.2021.158780>. /05/25/2021.
- [37] M. Almessiere, et al., Review on functional bi-component nanocomposites based on hard/soft ferrites: structural, magnetic, electrical and microwave absorption properties, *Nano-Struct. Nano-Obj.* 26 (2021), 100728, <https://doi.org/10.1016/j.nanos.2021.100728>.
- [38] X. Wang, Y. Lu, T. Zhu, S. Chang, W. Wang, CoFe2O4/N-doped reduced graphene oxide aerogels for high-performance microwave absorption, *Chem. Eng. J.* 388 (2020/05/15/2020), 124317, <https://doi.org/10.1016/j.cej.2020.124317>.
- [39] S. Yavari, N.M. Mahmodi, P. Teymouri, B. Shahmoradi, A. Maleki, Cobalt ferrite nanoparticles: preparation, characterization and anionic dye removal capability, *J. Taiwan Inst. Chem. Eng.* 59 (2016/02/01/2016) 320–329, <https://doi.org/10.1016/j.jtice.2015.08.011>.
- [40] H. Jiang, P. Yan, Q. Wang, S. Zang, J. Li, Q. Wang, High-performance Yb, N, P-tridoped anatase-TiO2 nano-photocatalyst with visible light response by sol-solvothermal method, *Chem. Eng. J.* 215 (2013) 348–357, <https://doi.org/10.1016/j.cej.2012.10.082>.
- [41] C. Namasivayam, D. Kavitha, Removal of Congo Red from water by adsorption onto activated carbon prepared from coir pith, an agricultural solid waste, *Dyes Pigments* 54 (1) (2002) 47–58, [https://doi.org/10.1016/S0143-7208\(02\)00025-6](https://doi.org/10.1016/S0143-7208(02)00025-6).
- [42] B.D. Venkatesan K, M. Bai, R. Supriya, R. Vidya, S. Madeswaran, P. Anandan, M. Arivanandhan, Y. Hayakawa, Structural and magnetic properties of cobalt-doped iron oxide nanoparticles prepared by solution combustion method for biomedical applications, *Int. J. Nanomed.* 10 (1) (2015) 189–198, <https://doi.org/10.2147/IJN.S82210>.
- [43] X. Meng, et al., Three-dimensional foam-like Fe3O4@C core-shell nanocomposites: controllable synthesis and wideband electromagnetic wave absorption properties, *J. Magn. Magn. Mater.* 502 (2020/05/15/2020), 166518, <https://doi.org/10.1016/j.jmmm.2020.166518>.
- [44] X. Meng, W. Lei, W. Yang, Y. Liu, Y. Yu, Fe3O4 nanoparticles coated with ultra-thin carbon layer for polarization-controlled microwave absorption performance, *J. Colloid Interface Sci.* 600 (2021/10/15/2021) 382–389, <https://doi.org/10.1016/j.jcis.2021.05.055>.
- [45] X. Meng, Y. Liu, G. Han, W. Yang, Y. Yu, Three-dimensional (Fe3O4/ZnO)@C Double-core@shell porous nanocomposites with enhanced broadband microwave absorption, *Carbon* 162 (2020/06/01/2020) 356–364, <https://doi.org/10.1016/j.carbon.2020.02.035>.